Stratospheric climate anomalies and ozone loss caused by the Hunga Tonga volcanic eruption

Xinyue Wang[1], William Randel[1], Yunqian Zhu[2], Simone Tilmes[1], Jon Starr[1], Wandi Yu[3], Rolando Garcia[1], Brian Toon[4], Mijeong Park[1], Douglas Kinnison[1], Adam Bourassa[5], Landon Rieger[5], and Jianghanyang Li[2]

[1]National Center for Atmospheric Research
[2]Cooperative Institute for Research in Environmental Sciences
[3]Hampton university
[4]University of Colorado Boulder
[5]University of Saskatchewan

December 7, 2022

Abstract

The Hunga Tonga-Hunga Ha'apai (HTHH) volcanic eruption in January 2022 injected extreme amounts of water vapor (H2O) and a moderate amount of the aerosol precursor (SO2) into the Southern Hemisphere (SH) stratosphere. The H2O and aerosol perturbations have persisted and resulted in large-scale SH stratospheric cooling, equatorward shift of the Antarctic polar vortex, and slowing of the Brewer-Dobson circulation associated with a substantial ozone reduction in the SH winter midlatitudes. Chemistry-climate model simulations forced by realistic HTHH inputs of H2O and SO2 reproduce the observed stratospheric cooling and circulation effects, demonstrating the observed behavior is due to the volcanic influences. Furthermore, the combination of aerosol transport to polar latitudes and a cold polar vortex enhances springtime Antarctic ozone loss, consistent with observed polar ozone behavior in 2022.

Stratospheric climate anomalies and ozone loss caused by the Hunga Tonga volcanic eruption

Authors: Xinyue Wang[1*], William Randel[1], Yunqian Zhu[2, 3 ,4], Simone Tilmes[1], Jon Starr[1], Wandi Yu[5], Rolando Garcia[1], Brian Toon[3, 6], Mijeong Park[1], Douglas Kinnison[1], Adam Bourassa[7], Landon Rieger[7], Jianghanyang Li[2, 8]

Affiliations:

[1]Atmospheric Chemistry Observations & Modeling lab, National Center for Atmospheric Research, Boulder, CO, USA

[2] Cooperative Institute for Research in Environmental Sciences, University of Colorado Boulder, Boulder, CO, USA, 80309

[3]Laboratory for Atmospheric and Space Physics, University of Colorado Boulder, Boulder, CO, USA

[4]Chemical Sciences Laboratory, National Oceanic and Atmospheric Administration, Boulder, CO, USA, 80305

[5]Department of Atmospheric and Planetary Sciences, Hampton university, VA, USA

[6]Department of Atmospheric and Oceanic Sciences, University of Colorado Boulder, Boulder, CO, USA

[7]Institute of Space and Atmospheric Studies, University of Saskatchewan, Saskatoon, SK, Canada

[8]Global Monitoring Laboratory, National Oceanic and Atmospheric Administration, Boulder, CO, USA, 80305

*Corresponding author. Email: xinyuew@ucar.edu

Abstract: The Hunga Tonga-Hunga Ha'apai (HTHH) volcanic eruption in January 2022 injected extreme amounts of water vapor (H_2O) and a moderate amount of the aerosol precursor (SO_2) into the Southern Hemisphere (SH) stratosphere. The H_2O and aerosol perturbations have persisted and resulted in large-scale SH stratospheric cooling, equatorward shift of the Antarctic polar vortex, and slowing of the Brewer-Dobson circulation associated with a substantial ozone reduction in the SH winter midlatitudes. Chemistry-climate model simulations forced by realistic HTHH inputs of H_2O and SO_2 reproduce the observed stratospheric cooling and circulation effects, demonstrating the observed behavior is due to the volcanic influences. Furthermore, the combination of aerosol transport to polar latitudes and a cold polar vortex enhances springtime Antarctic ozone loss, consistent with observed polar ozone behavior in 2022.

One-Sentence Summary: The HTHH volcanic eruption changed stratospheric temperatures and circulation and caused midlatitude and polar ozone losses.

Global ozone levels are recovering due to reductions of CFCs in the stratosphere as the result of the Montreal Protocol and its amendments. However, natural impacts from wildfires (1, 2) or from large volcanic eruptions (3), can temporarily impact stratospheric ozone. The Hunga Tonga-Hunga Ha'apai (HTHH) submarine volcano erupted on 15th January 2022 and increased the global stratospheric water burden by ~10%, setting a record since the modern satellite era and differentiating itself from previous major volcanic eruptions (4-6). The excess moisture is expected to remain in the stratosphere for several years and could exert a substantial impact on the climate system (7, 8). A moderate amount of sulfur-containing gases, approximately 0.4-0.5 Tg (9), was lofted into the stratosphere after the HTHH eruption which quickly converted to sulfate aerosol particles (10). Simulations of the Whole Atmosphere Community Climate Model (WACCM), a coupled chemistry-climate model described under Methods in the supplementary material, suggest the excessive moisture halves the SO_2 lifetime and promotes faster sulfate aerosol formation, resulting in large perturbations to stratospheric aerosol evolution (10). Our work documents unprecedented changes in stratospheric climate and ozone caused by this water vapor-rich volcanic eruption that continues to influence the Earth system.

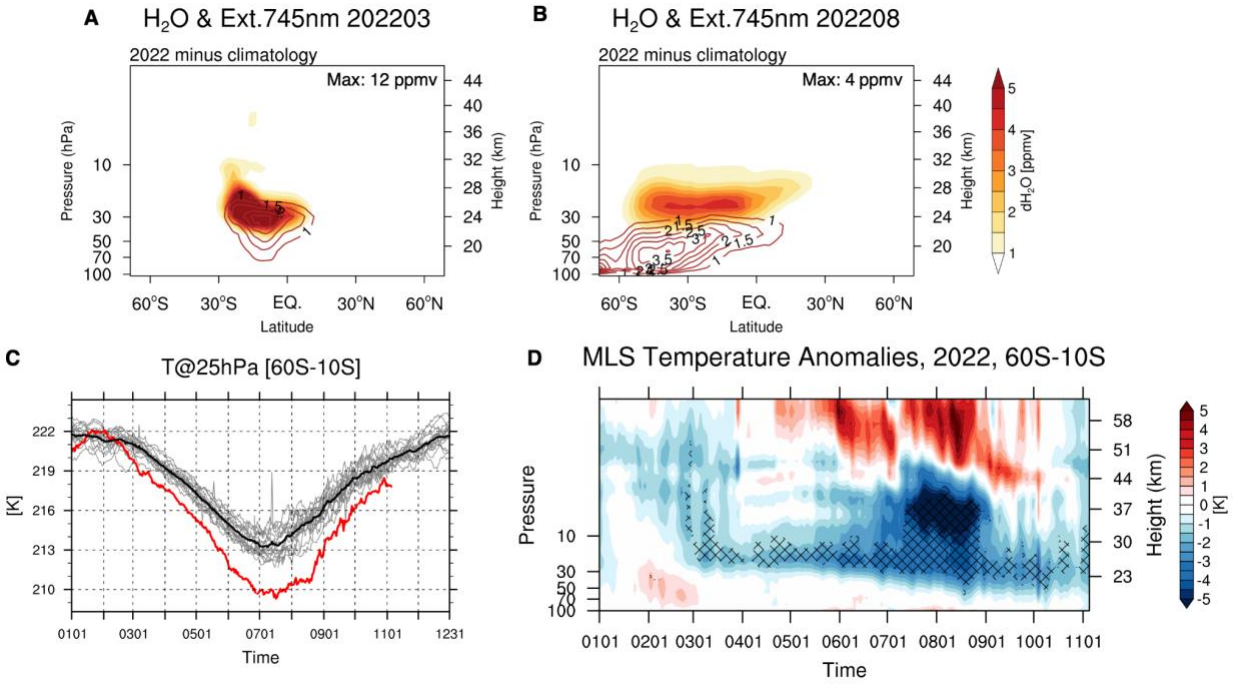

Fig. 1. Observed perturbations after the HTHH eruption. (**A** and **B**) Dispersion of the HTHH H_2O and aerosol plumes between March and August 2022. H_2O anomalies (colors, ppmv) are derived from the Aura Microwave Limb Sounder (MLS) data and calculated as deviations from the 2004-2021 background. The maximum increase is indicated by the number on the top right corner. Aerosol is quantified by the Ozone Mapping and Profiler Suite Limb Profiler (OMPS-LP) aerosol extinction at 745 nm (red contours, 10^{-3} km^{-1}). (**C** and **D**) Anomalous stratospheric temperature changes in the SH during 2022. (**C**) Temperatures at 25 hPa over 60°S-10°S from MLS observations showing persistent anomalous cooling in 2022 (red line). (**D**) Temperature anomalies

in 2022 over 60°S-10°S as a function of altitude and time, calculated as the difference from the average over 2004-2021. Hatched regions in (**D)** indicate where the 2022 anomalies are outside the range of all variability during 2004-2021.

Increased stratospheric H_2O acts to cool the stratosphere (11, 12), while enhanced aerosols lead to stratospheric warming, and these combined effects are expected to modify stratospheric climate. Satellite observations show that the HTHH H_2O and aerosol plumes have persisted in the stratosphere and evolved over several months (Figs. 1A and B). The majority of the sulfate aerosol was initially colocated with the H_2O plume near 24 km (March 2022 in Fig. 1A), but has subsequently sedimented to the lower stratosphere and dispersed in latitude to span the entire Southern Hemisphere (SH, August 2022 in Fig. 1B). The H_2O plume was centered near 25 km and covered 60°S-20°N by August 2022; the H_2O anomalies (>4 ppmv in Fig. 1B) are large compared to the stratospheric background of ~5 ppmv.

Satellite observations also show evidence of systematic stratospheric temperature changes following the HTHH eruption (Figs. 1C and D). Temperatures near 25 hPa over the SH show cold anomalies in 2022 that are well outside of previous variability, beginning one-to-two months after the eruption (Fig. 1C). The time scale is consistent with a radiative response to the increased H_2O near this altitude (12). The vertical structure of the temperature anomalies averaged over 60°S-10°S shows cooling covering much of the mid stratosphere with distinctive time evolution (Fig. 1D). Cold anomalies occur over the depth of the stratosphere (~25-55 km) from late January-March, overlaying warm maxima in the lower stratosphere (~18-25 km). There are persistent cold anomalies centered near 25 km throughout 2022 (overlapping the H_2O plume), and the anomalies grow in magnitude and extend up to ~40 km during the SH winter (June-August). During these months there are anomalous warm temperatures above 45 km.

Cold temperature anomalies during SH winter occur in high latitudes, centered near 50°S, and do not directly overlap the H_2O plume (Fig. 2A). High latitude cold anomalies (in excess of 15 K) occur in combination with warm tropical anomalies, with maxima near 23 and 38 km. Part of the temperature maximum is related to the phase of the Quasi-Biennial Oscillation (QBO) in 2022. The latitudinal see-saw patterns are suggestive of coupling to the hemispheric-scale mean circulation (13). The strong high latitude temperature anomalies are in balance with changes in the polar vortex zonal winds (Fig. 3A), which show intensification and equatorward shift throughout the winter.

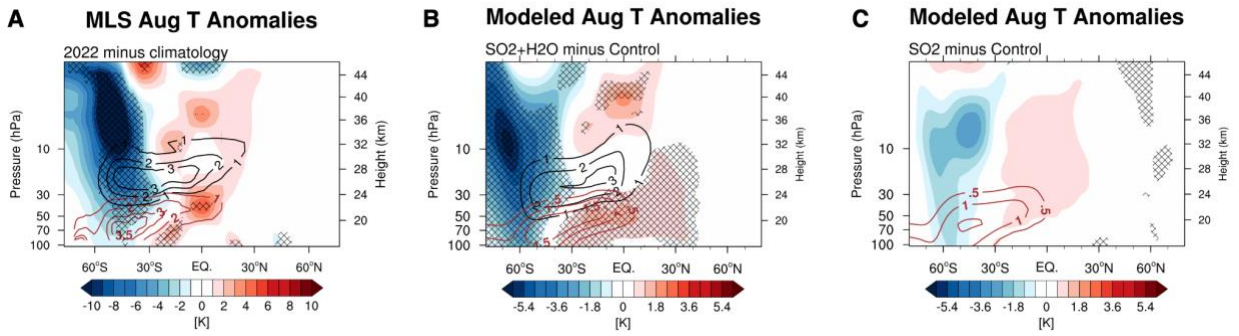

Fig. 2. Observed and modeled temperature anomalies in August 2022 (color shading, K). (**A**) MLS observations, calculated as differences between the 2022 and the 2004-2021 average. Hatched regions in (**A)** indicate where the 2022 anomalies are outside the range of all variability during 2004-2021. Panel (**B** and **C**) show WACCM simulated modeled temperature changes in all-forcing (H_2O+SO_2) and SO_2 only (SO_2) simulations, compared to no-forcing control runs. Red line contours denote the aerosol extinction in 10^{-3} km^{-1}, and black line contours denote the anomalous H_2O concentration in ppmv. Hatched regions mark the grid points for which the changes exceed the 95% significance level according to Student's *t*-test.

The unprecedented evolution of temperatures and circulation in 2022 suggests forced changes from the HTHH eruption, but also contains components of internal variability. To evaluate these effects, we have simulated impacts of the HTHH H_2O and aerosol plumes using ensemble simulations of WACCM (14) with and without the volcanic injections. The model uses injections consistent with observed HTHH H_2O and SO_2 estimates in January 2022 (with SO_2 converting to sulfate aerosol). The model was constrained by winds and temperatures from meteorological analyses (see Methods) for the first two weeks of simulation, and was free-running afterwards. We use 10-member ensemble simulations of the combined effects of (H_2O+SO_2) compared to control simulations (no HTHH input), along with simulations of separate H_2O and SO_2 inputs (see Methods).

The modeled evolution of the H_2O and sulfate aerosol plumes in the H_2O+SO_2 case during 2022 are similar to those observed. The plumes initially overlap and then separate vertically over time (Fig. 2B), with latitudinal dispersion similar to observed behavior (15, Figs. 1A and B). The aerosol layer in the lower stratosphere extends to polar latitudes near the bottom of the polar vortex, while the H_2O plume spreads poleward with the QBO secondary circulation but is mostly excluded from polar latitudes by the stronger jet near 25 km. The modeled structure of temperature changes in the (H_2O+SO_2) simulations capture the observed behavior with surprising detail (Figs. 1D and S1), including cooling anomalies that increase in magnitude during SH winter and couple to the changes in high latitude polar vortex. The simulated zonal wind changes show a strengthening and equatorward shift of the winter polar vortex in response to the (H_2O+SO_2) forcing (Fig. 3B), in remarkable agreement to observed behavior (Fig. 3A). The model (and observations) show that the strengthened polar vortex persists into SH spring (Figs. S4 and S5). The temperature changes are in balance with anomalies in the overturning Brewer-Dobson circulation (BDC, Fig. 3B) The

BDC anomalies include high latitude upwelling and low latitude downwelling that opposes and weakens the normal background, equator to pole circulation. The anomalies in the BDC are consistent with weakened planetary-scale wave forcing (resolved EP flux divergence) in the model. There are vertical out-of-phase temperature changes above 45 km (Figs. 1D, S1-S3) that are characteristic of dynamically forced effects (16).

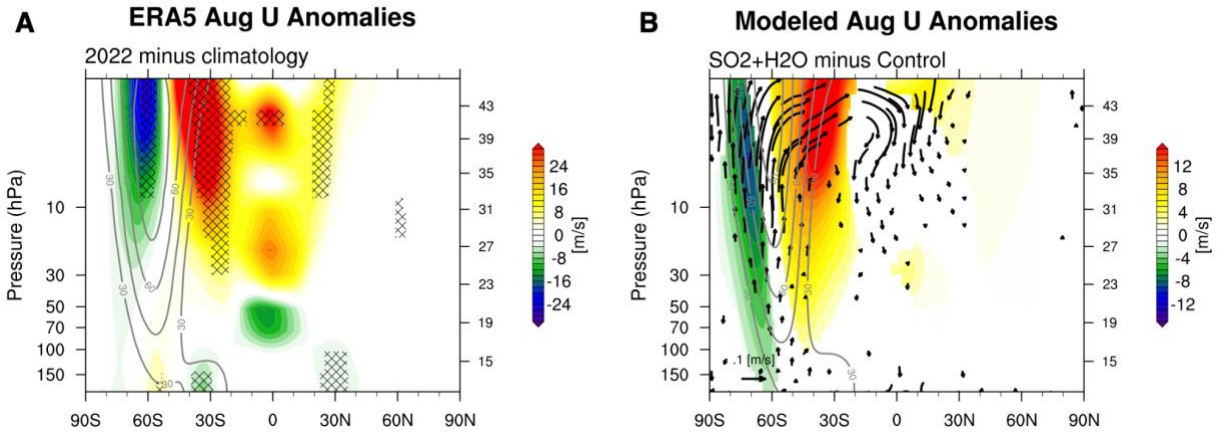

Fig. 3. Anomalous zonal wind changes in August 2022. Colors show zonal mean zonal wind anomalies in (**A**) observations from the ERA5 reanalysis data and (**B**) simulations in the all-forcing (H_2O+SO_2) case compared to the control runs. Gray contours show the background zonal winds with an interval of 15 m/s. The vectors in (**B**) depict anomalies in the simulated residual mean meridional circulation (BDC). Hatched regions in (**A)** indicate where the 2022 anomalies are outside the range of all variability during 2004-2021. Regions where anomalies are not significant at the 95% level are shaded white.

Modeled temperature changes with only SO_2 (sulfate aerosol) forcing (Fig. 2C) are similar to changes under total (H_2O+SO_2) forcing but are weaker and mostly not significant, implying that enhanced H_2O has amplified stratospheric cooling and polar vortex strengthening in the high latitudes. Without H_2O injection the volcanic aerosol layer is thicker and heats the lower stratosphere over a deeper vertical layer. In contrast, the enhanced H_2O plume (Fig. 2B) produces local cooling that is sandwiched vertically between tropical warming anomalies, with similar patterns to those observed (Fig. 2A). Model simulations with only H_2O forcing show a very different circulation response, with a weakened polar vortex and enhanced BDC. We conclude that including both H_2O and SO_2 (sulfate aerosol) forcings are important for realistic simulation of the HTHH responses, and that there is strong coupling between these separate forcings.

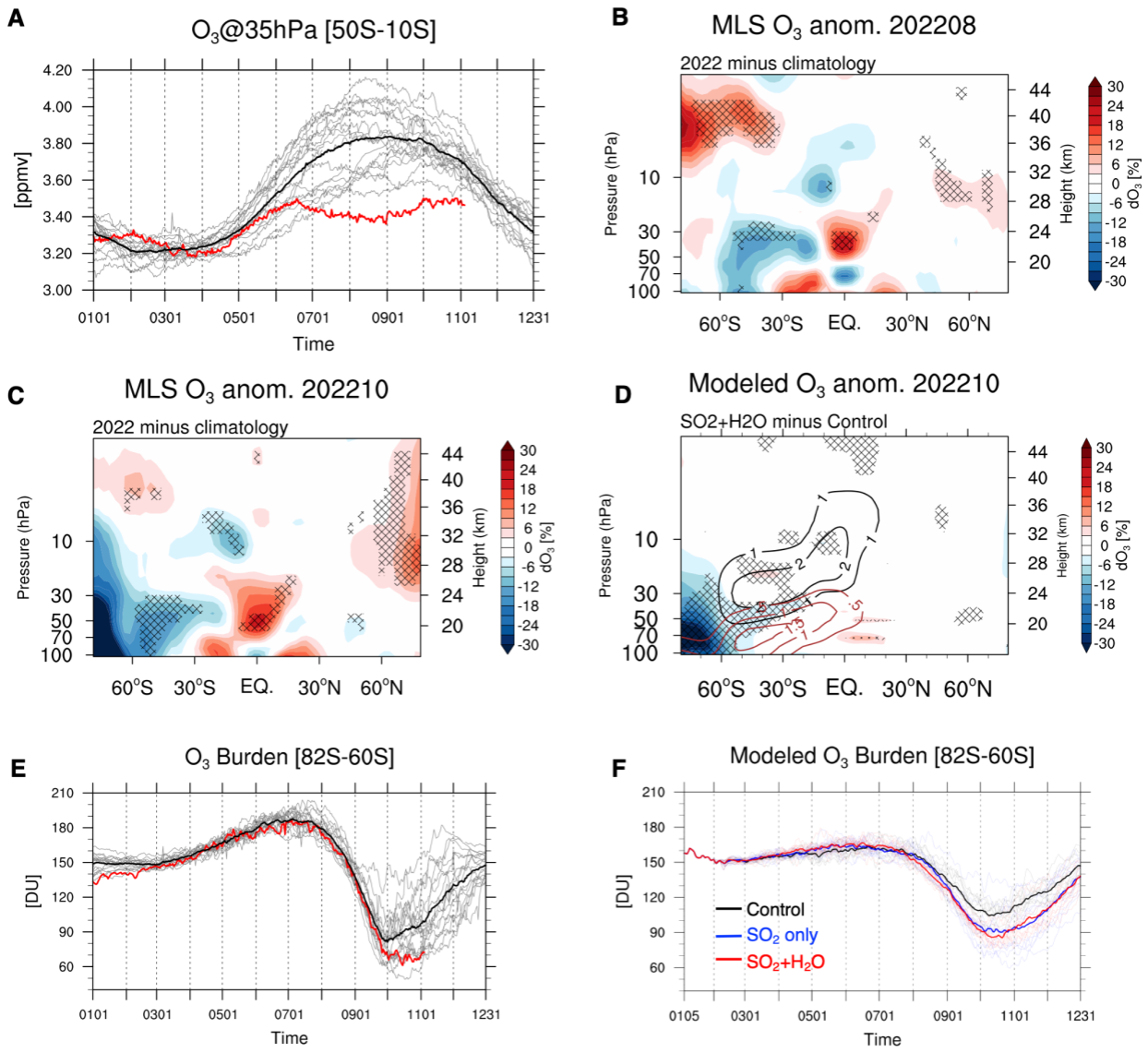

Fig. 4 Evolution of stratospheric ozone after HTHH. (**A**) Time series of MLS observed ozone at 35 hPa, 50°S-10°S, showing large ozone depletion in 2022 (red line). (**B, C**) Fractional ozone anomalies (%) from MLS in August and October 2022, respectively. Hatched regions in (**B, C**) indicate where the 2022 anomalies are outside the range of all variability during 2004-2021. (**D**) Modeled October ozone changes in H_2O+SO_2 minus control simulations. Hatched regions mark the grid points for which the changes exceed the 95% significance level according to Student *t*-test. (**E**) MLS observations of polar cap (82°S-60°S) ozone column over 11-22 km in 2004-2022, and (**F**) corresponding modeled results comparing control, H_2O+SO_2 and SO_2 only simulations.

Stratospheric ozone changes after HTHH can be anticipated from both circulation effects and anomalous chemistry from enhanced H_2O and aerosols. MLS observations show lower stratospheric (LS) ozone reductions during winter over the SH midlatitudes and tropics (~50°S-10°S) that are outside of previous variability (Figs. 4A and B). The SH mid-latitude ozone

reduction in August is reproduced in the model (Fig. S6) and is proved to be mainly linked to circulation effects, rather than the chlorine-catalyzed mid-latitude ozone depletion seen after previous explosive volcanic eruptions (17). The wintertime ozone losses in the LS (35 hPa, Fig. 4A) are a fingerprint of the anomalous winter circulation changes identified above (Fig. 3B). We see consistent behavior between ozone as shown in Figure 4B and anomalies in N_2O, an inactive trace species with tropospheric source, with an enhancement in the SH midlatitudes and a reduction in the tropics (Fig. S7). The model also highlights chemical ozone effects at higher altitudes (above 10 hPa) tied to changes in NO_x and HO_x radical species (Figs. S6C and D), but the net ozone impacts are relatively small (Fig. S6B).

Further large ozone losses occur associated with the Antarctic ozone hole (Figs. 4C and E), where variability is tied to polar stratospheric cloud (PSC) and aerosol amounts together with cold temperatures that generate photochemically active chlorine (18). Polar ozone losses are enhanced by HTHH aerosols that reach the polar stratosphere, in combination with relatively cold temperatures from circulation effects that enhance reactive chlorine chemistry (Fig. 4D and S7D). Strong influence of these effects is seen in the modeled springtime polar ozone evolution (Fig. 4F), where the combined effects of H_2O+SO_2 lead to net losses of ~15 DU compared to control runs amid substantial variability. Comparisons with SO_2 only simulations (blue lines in Fig. 4F) show that most of the polar ozone losses are due to the HTHH aerosols, with effects enhanced by the H_2O plume and associated circulation effects. Observations show high polar aerosol amounts (Fig. S9) and large and persistent springtime polar ozone depletions in 2022 (Fig. 4E). The low 2022 ozone hole amounts are rivaled by other recent years with enhanced polar aerosols due to volcanic eruptions (Calbuco volcanic eruption in 2015, 3) and smoke from wildfires (bush fires in 2020 and persisting to 2021, 19, Fig. S9). The anomalous low polar ozone in 2022 is interpreted in light of the model simulations (Fig. 4F) as being a direct effect of HTHH. Because springtime polar temperatures and vortex persistence are closely linked to polar ozone amounts (19), we anticipate a cold and prolonged polar vortex persisting into December 2022.

Satellite measurements demonstrate persistent perturbations in stratospheric temperatures and circulation following the HTHH eruption, including influences on the seasonally-evolving polar vortex and BDC. These changes led to anomalies in stratospheric climate tied to HTHH. Global chemistry-climate model simulations forced by HTHH inputs can track the evolving H_2O and aerosol plumes, and the modeled volcanic responses in temperatures and circulation are similar to the time-evolving patterns of the observed behavior. This agreement demonstrates that the observed stratospheric changes are a fingerprint of the forced global-scale response to the HTHH eruption, and sensitivity experiments demonstrate that the combined effects of both H_2O and SO_2 (sulfate aerosol) are important. Forced circulation changes result in anomalous low ozone in the SH winter midlatitude lower stratosphere. Furthermore, aerosol transport to the Antarctic lower stratosphere combined with a circulation-induced cold polar vortex results in large and persistent Antarctic ozone losses in the model, mimicking the low polar ozone observed in 2022. These 2022 SH ozone losses caused by HTHH are transient effects and should not impact the long-term ozone recovery expected from the Montreal Protocol. The HTHH eruption provides a remarkable natural

experiment for validating a fully coupled chemistry-climate model and provides confidence in ensemble forecast simulations, such as those performed here.

References:

1. Bernath, P., Boone, C. & Crouse, J. Wildfire smoke destroys stratospheric ozone. Science (80-.). 375, 1292–1295 (2022).
2. Solomon, S. *et al.* On the stratospheric chemistry of midlatitude wildfire smoke. *Proc. Natl. Acad. Sci.* **119**, e2117325119 (2022).
3. Stone, K. A. *et al.* Observing the impact of Calbuco volcanic aerosols on South Polar ozone depletion in 2015. *J. Geophys. Res. Atmos.* **122**, 11–862 (2017).
4. Vömel, H., Evan, S. & Tully, M. Water vapor injection into the stratosphere by Hunga Tonga-Hunga Ha'apai. Science (80-.). 377, 1444–1447 (2022).
5. Khaykin, S. et al. Global perturbation of stratospheric water and aerosol burden by Hunga eruption. (2022).
6. Millán, L. et al. The Hunga Tonga-Hunga Ha'apai Hydration of the Stratosphere. (2022).
7. Solomon, S. *et al.* Contributions of stratospheric water vapor to decadal changes in the rate of global warming. *Science (80-.).* **327**, 1219–1223 (2010).
8. Li, F. & Newman, P. Stratospheric water vapor feedback and its climate impacts in the coupled atmosphere–ocean Goddard Earth Observing System Chemistry-Climate Model. *Clim. Dyn.* **55**, 1585–1595 (2020).
9. Carn, S., Krotkov, N., Fisher, B. & Li, C. Out of the blue: volcanic SO_2 emissions during the 2021-2022 Hunga Tonga-Hunga Ha'apai eruptions. (2022).
10. Zhu, Y. *et al.* Perturbations in stratospheric aerosol evolution due to the water-rich plume of the 2022 Hunga-Tonga eruption. *Commun. Earth Environ.* **3**, 1–7 (2022).
11. de F, F., Piers, M. & Shine, K. P. Stratospheric water vapour changes as a possible contributor to observed stratospheric cooling. Geophys. Res. Lett. 26, 3309–3312 (1999).
12. Sellitto, P. et al. The unexpected radiative impact of the Hunga Tonga eruption of January 15th, 2022. (2022).
13. Yulaeva, E., Holton, J. R. & Wallace, J. M. On the cause of the annual cycle in tropical lower-stratospheric temperatures. J. Atmos. Sci. 51, 169–174 (1994).
14. Gettelman, A. et al. The whole atmosphere community climate model version 6 (WACCM6). J. Geophys. Res. Atmos. 124, 12380–12403 (2019).
15. Schoeberl, M. R. et al. Analysis and impact of the Hunga Tonga-Hunga Ha'apai Stratospheric Water Vapor Plume. Geophys. Res. Lett. n/a, e2022GL100248.
16. Andrews, D. G., J. R. Holton, and C. B. Leovy, Middle Atmospheric Dynamics, 489 pp., Academic, San Diego, Calif., (1987).
17. Hofmann, D. J. & Solomon, S. Ozone destruction through heterogeneous chemistry following the eruption of El Chichon. J. Geophys. Res. Atmos. 94, 5029–5041 (1989).
18. Solomon, S., Garcia, R. R., Rowland, F. S. & Wuebbles, D. J. On the depletion of Antarctic ozone. Nature 321, 755–758 (1986).

19. Rieger, L. A., Randel, W. J., Bourassa, A. E. & Solomon, S. Stratospheric temperature and ozone anomalies associated with the 2020 Australian new year fires. Geophys. Res. Lett. 48, e2021GL095898 (2021).
20. Richter, J. H. et al. Subseasonal Earth system prediction with CESM2. Weather Forecast. 37, 797–815 (2022).
21. Livesey, N. J. *et al.* Version 5.0 x level 2 and 3 data quality and description document (Tech. Rep. No. JPL D-105336 Rev. A). *Jet Propuls. Lab.* (2020).
22. Zawada, D. J., Rieger, L. A., Bourassa, A. E., & Degenstein, D. A. Tomographic retrievals of ozone with the OMPS Limb Profiler: algorithm description and preliminary results. Atmospheric Measurement Techniques, 11(4), 2375-2393 (2018).

Supplementary Materials for

Stratospheric climate anomalies and ozone loss caused by the Hunga Tonga volcanic eruption

Methods

We use the Community Earth System Model version 2 (CESM2) WACCM to simulate the stratospheric H_2O and aerosol enhancements due to the HTHH eruption, and evaluate their influence on stratospheric temperature, circulation and ozone chemistry. WACCM has 70 vertical layers extending upward to 140 km with vertical resolution about 1 to 1.5 km in the stratosphere. The model is fully coupled to an interactive ocean, sea-ice, and land, and initialized in the beginning of January by the observed sea-surface temperatures similar to that described in (20). The HTHH volcanic H_2O (~ 150 Tg) and sulfur dioxide (SO_2 ~0.42 Tg) are injected on January 15, 2022 from ~20 to 35 km (details in 10). To accurately simulate the early plume structure and evolution, WACCM winds and temperatures are nudged to GEOS5 meteorological analysis throughout January 2022. After February 1, 2022 the simulations are free-running to simulate fully-coupled variability including the coupling between changes in composition and radiation. We conducted four sets of experiments: the control case without SO_2 or H_2O (no volcanic forcing); an SO_2 only case with only SO_2 injection; an H_2O only case with only H_2O injection, and the SO_2+H_2O case with both SO_2 and H_2O injection, which mimics the total forcing of HTHH eruption. We run ten ensembles for each scenario to examine internal variability and isolate forced behavior. Individual ensemble members differed by the last date of the meteorological nudging, around February 1st, 2022.

The aerosol extinction simulated in the model is about 60% of the observed values after two months of the eruption (10), which can be improved in the future by including more detailed microphysical processes of aerosol formation and adding pre-existing particles for volcanic gases to condense on, such as volcanic ashes. The simulated changes in temperature, wind, and ozone are about half as large as the observed magnitudes (e.g. Fig. 3). The low bias may come from comparing 2022 minus climatology in observations with 2022 minus no volcano simulation in the model where the impact of internal variability is not included. In spite of these caveats, the key

features of observed changes can be reproduced by our model simulation, suggesting that these patterns are largely due to volcanic forcing following HTHH.

The MLS instrument was launched onboard the EOS Aura satellite in 2004 as part of the "A-Train" satellite constellation and has operated continuously since in a low-earth, high-latitude, sun-synchronous orbit. The instrument utilizes five broad channels, with centers ranging approximately from 118-2500 GHz, in a limb-viewing configuration to measure various atmospheric properties and constituents, such as temperature, O_3, N_2O, and NO. For this work, version 5.0 of MLS water vapor, ozone, and temperature data (21) were compiled into a daily zonal means at a resolution of 2.5° latitude.

Aerosol extinction data is from the USASK OMPS Limb Profiler product (22). This uses the center of the three slits to retrieve aerosol at 745 nm with a tomographic inversion. The tomographic product improves resolution and reduces artifacts from spatially inhomogeneous aerosols. However, the retrieval still relies on assumed aerosol size and optical properties that may cause biases during periods of enhanced aerosol and contribute to differences with the modeled aerosol.

Figs. S1-S9

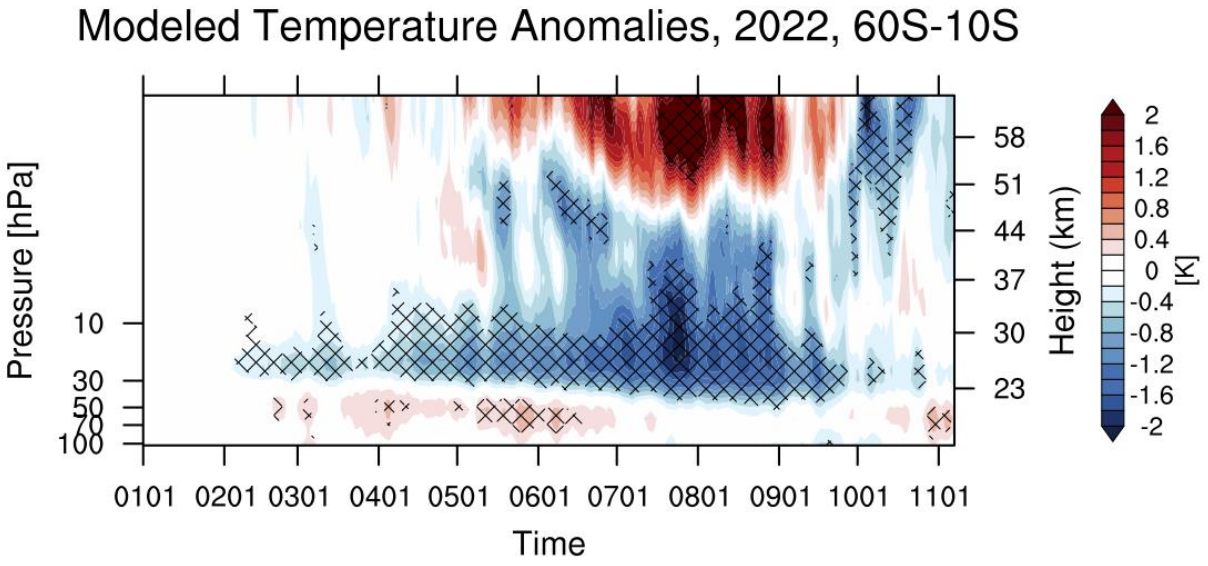

Fig. S1 Modeled temperature changes over 60°S-10°S as a function of altitude and time, calculated as the difference from all-forcing (H_2O+SO_2) and no-forcing control runs. Hatched regions mark the grid points for which the changes exceed the 95% significance level according to Student *t*-test.

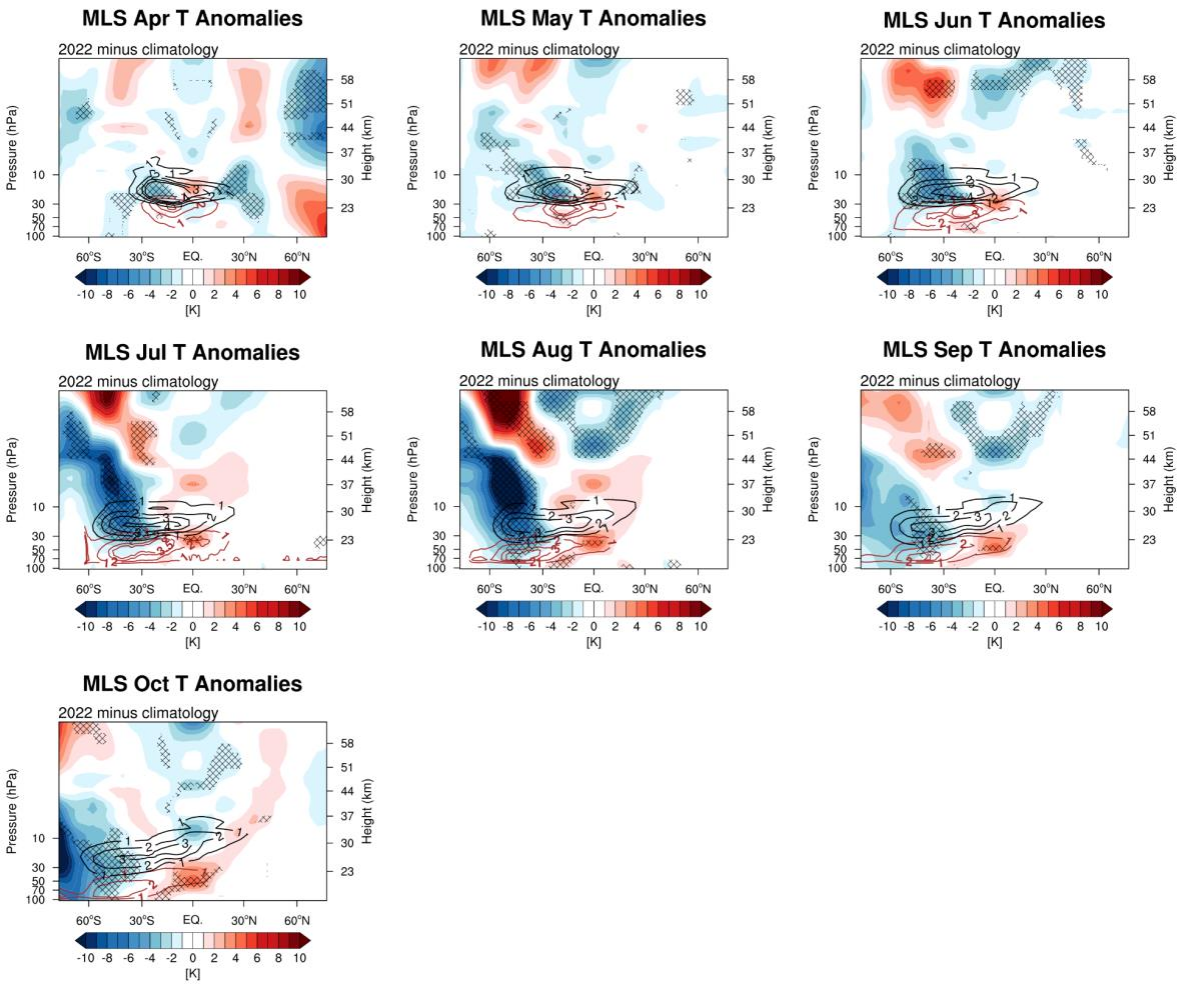

Fig. S2 Evolutions of MLS temperature anomalies (difference from the 2004-2021 climatology) from April to October 2022. Hatched regions indicate where the 2022 anomalies are outside the range of all variability during 2004-2021. Red contours denote the OMPS-LP aerosol extinction in 10^{-3} km^{-1}, and black contours denote the anomalous H_2O concentration in ppmv.

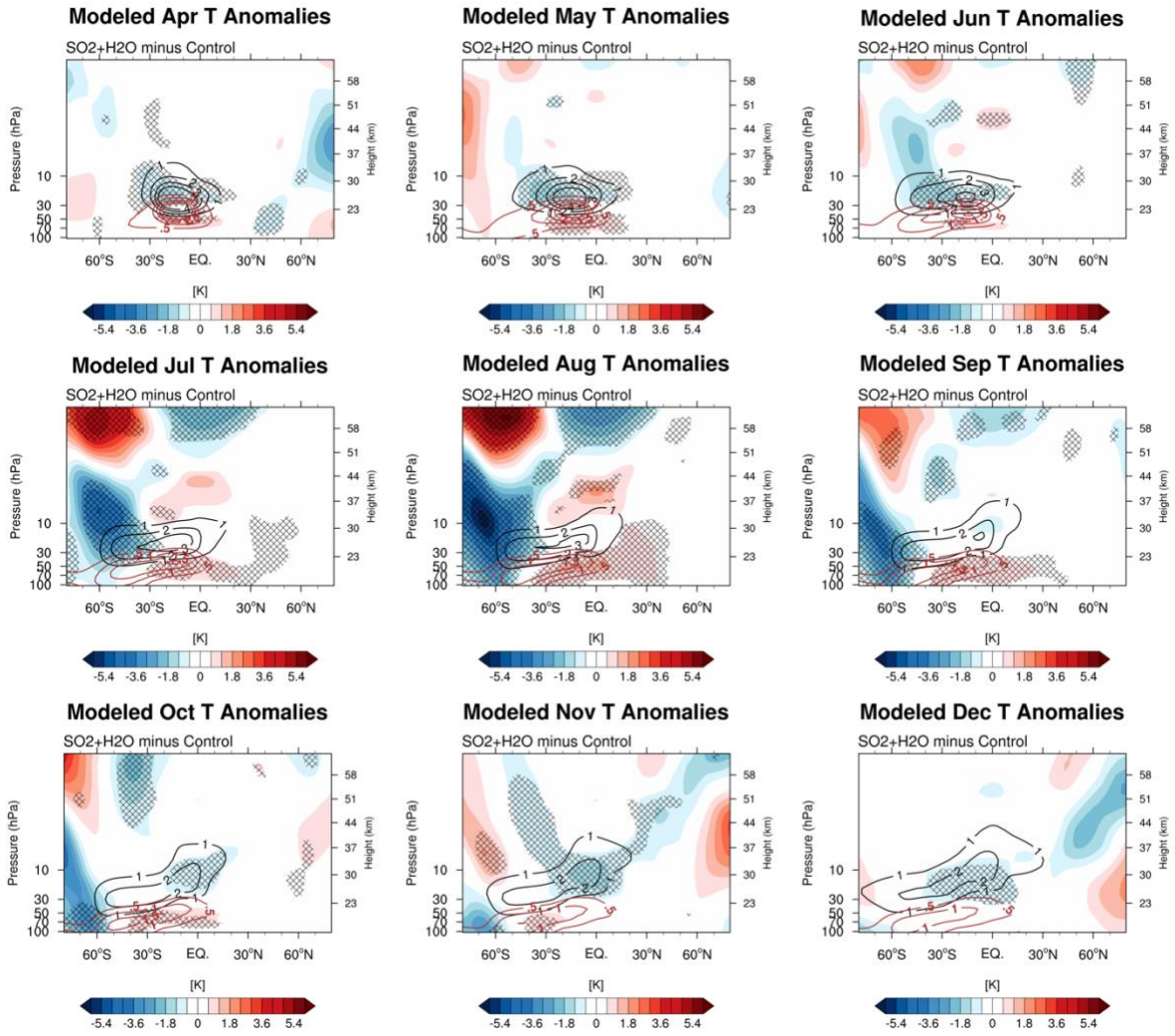

Fig. S3 Evolutions of WACCM simulated temperature changes (SO_2+H_2O simulations minus control runs) from April to December. During April, May and June, the cold temperature anomalies collocate with the water plume, showing a direct response from water vapor diabatic cooling effect. From July to October, a strong cooling occurs from 90° to ~40°S, from tropopause to 50 km, which is due to dynamic response to the volcanic injections (explained in the main text).

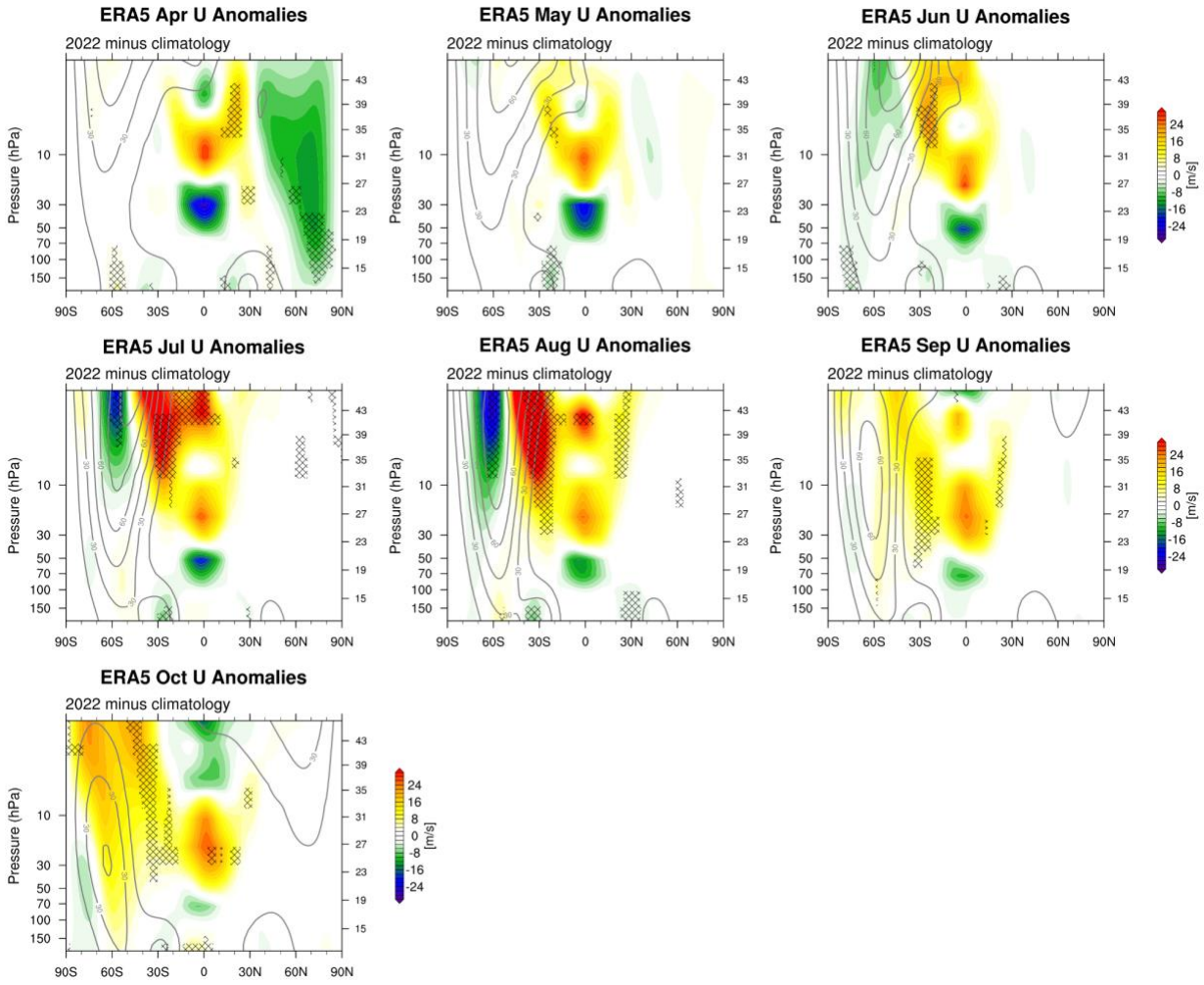

Fig. S4 Colors show zonal wind anomalies (differences from 2004-2021 climatology) from April to October 2022 in ERA5 reanalysis data. Gray contours show the background zonal winds with an interval of 15 m/s. Hatched regions indicate where the 2022 anomalies are outside the range of all variability during 2004-2021.

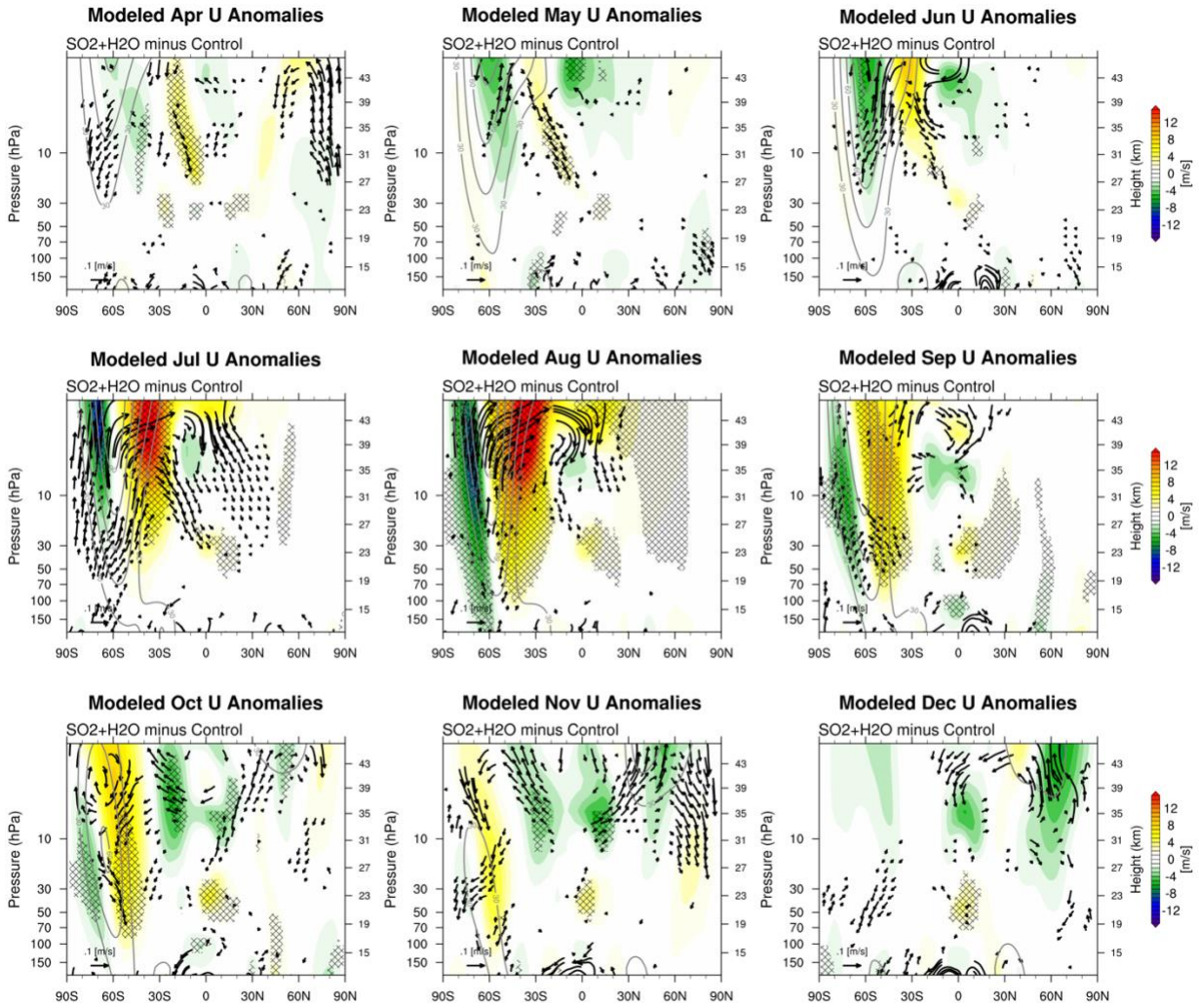

Fig. S5 Modeled zonal wind changes from April to December, calculated as the difference between all-forcing (H_2O+SO_2) simulations and the control runs. Gray contours show the background zonal winds with an interval of 15 m/s. The vectors depict anomalies in the simulated residual mean meridional circulation (BDC). Regions where changes are significant at the 95% level are hatched.

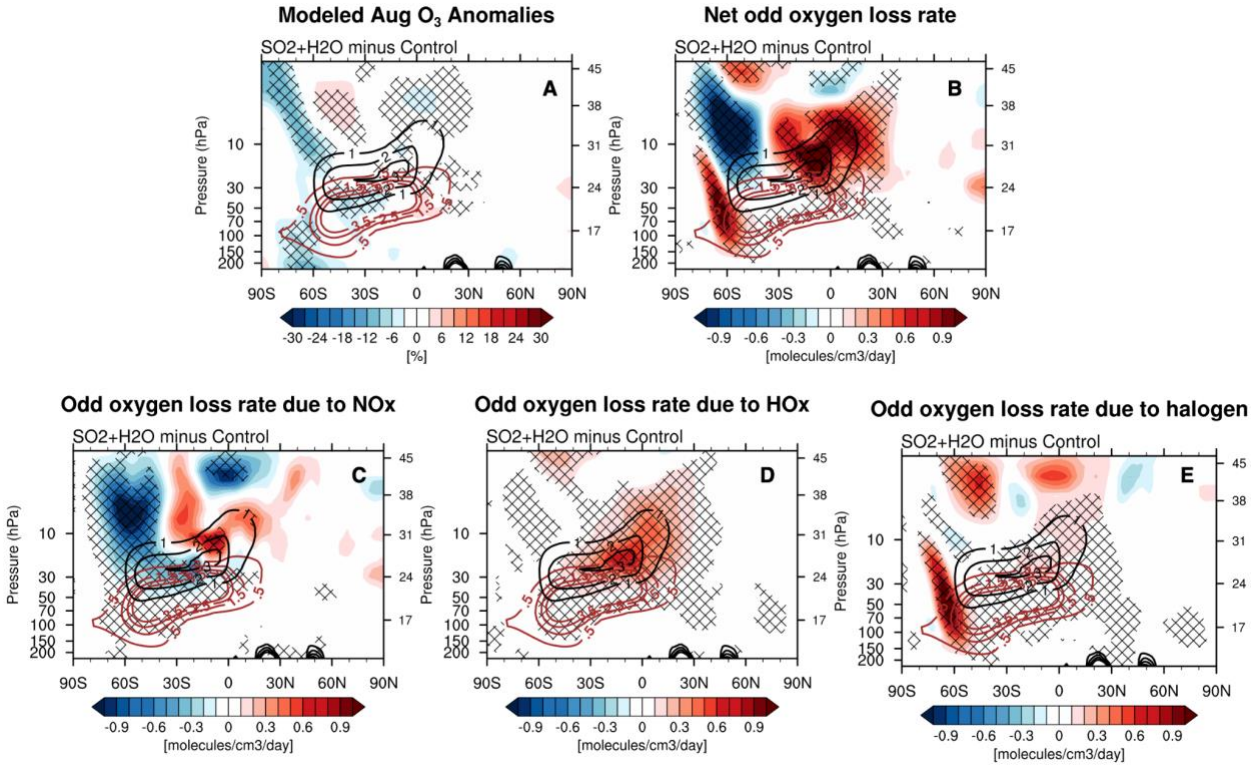

Fig. S6 (**A**) Simulated fractional ozone anomalies in August 2022 (color shading, %). (**B**) Net odd oxygen loss rate due to chemistry processes (color shading, molecules cm^{-3} day^{-1}). Odd oxygen loss rate due to (**C**) NO_x cycle, (**D**) HO_x cycle, and (**E**) halogen cycles. Regions where chemistry is important the positive loss rate anomalies (in red shading) coincide with the negative ozone anomalies (in blue shading). Red line contours denote the aerosol concentration in ppbv, and black line contours denote the anomalous H_2O concentration in ppmv. Regions where changes are significant at the 95% level are hatched.

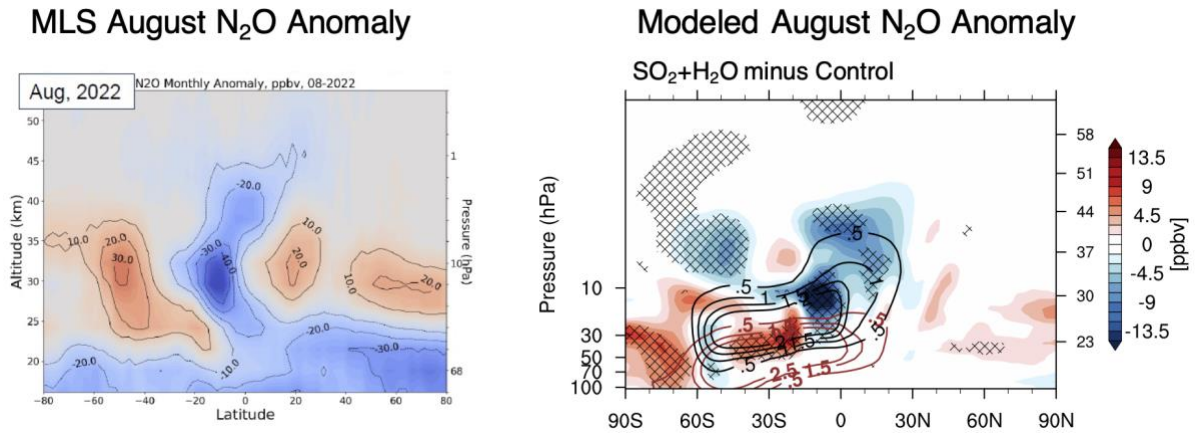

Fig. S7 (**A**) MLS August N_2O anomalies (ppbv) in August 2022, calculated as deviation from the 2004-2021 climatology. (**B**) WACCM simulated August N_2O anomalies (ppbv) in SO_2+H_2O minus control runs. Red contours denote the aerosol concentration in ppbv, and black contours

denote the anomalous H_2O concentration in ppmv. Regions where changes are significant at the 95% level are hatched.

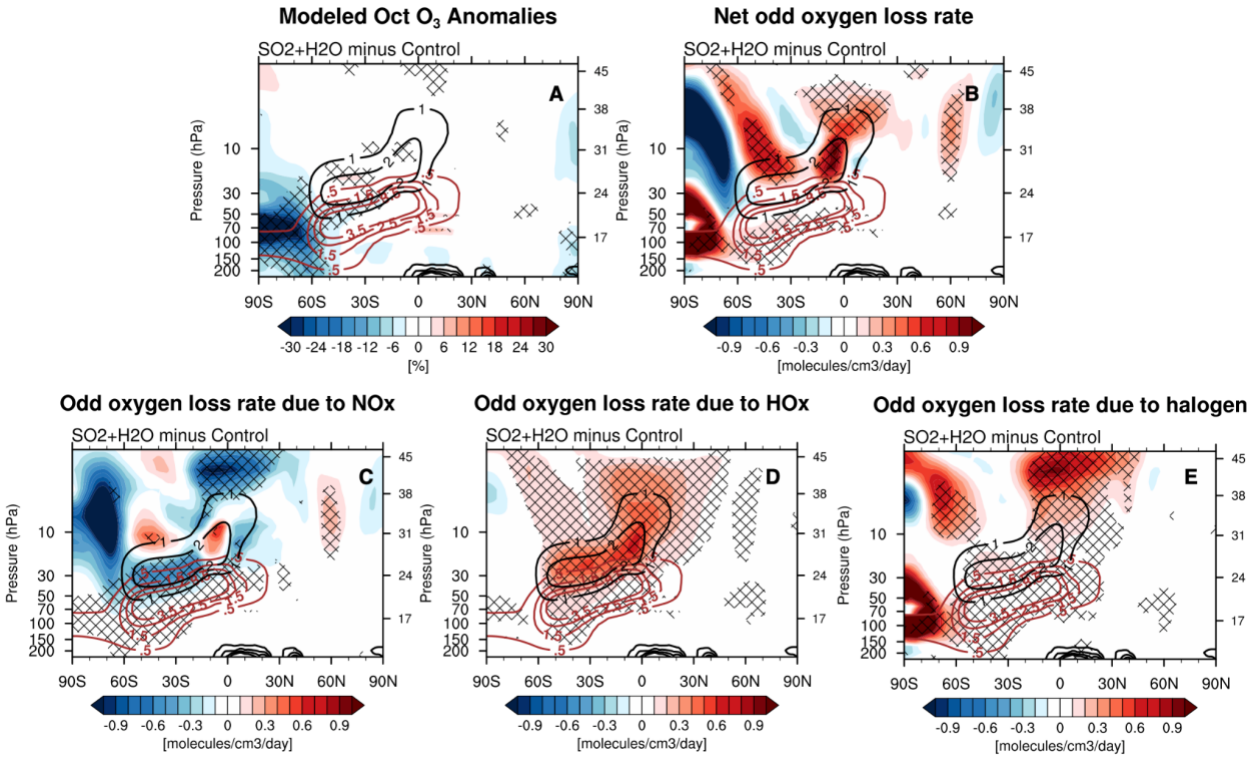

Fig. S8 (**A**) Simulated fractional ozone anomalies in October 2022 (color shading, %). (**B**) Net odd oxygen loss rate due to chemistry processes. Odd oxygen loss rate due to (**C**) NOx cycle, (**D**) HOx cycle, and (**E**) halogen cycles. Red line contours denote the aerosol concentration in ppbv, and black line contours denote the anomalous H_2O concentration in ppmv. Regions where changes are significant at the 95% level are hatched.

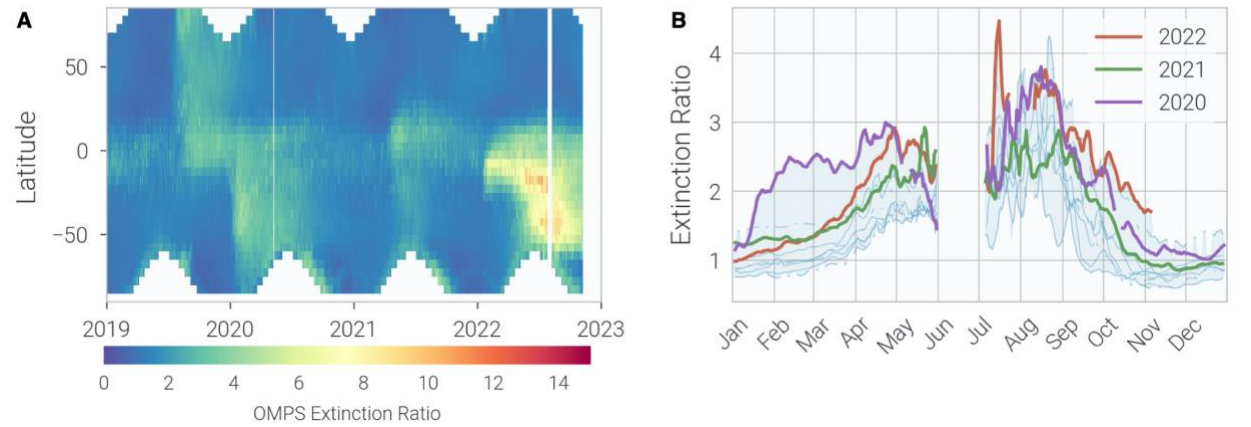

Fig. S9 (**A**) Latitude versus time section of OMPS-LP lower stratosphere aerosol extinction over 13 km - 22.5 km. (**B**) Time series of aerosol extinction for each year over 2012-2022 between 90° to ~60°S over the same altitudes.

Acknowledgments
X.W. is supported by the NSF via NCAR's Advanced Study Program Postdoctoral Fellowship. This project received funding from NOAA's Earth Radiation Budget (ERB) Initiative (CPO #03-01-07-001). This research was supported in part by NOAA cooperative agreements NA17OAR4320101 and NA22OAR4320151, and by the NASA Aura Science Team under Grant 80NSSC20K0928. The authors thank Drs Nathaniel Livesey, Michelle Santee, Paul Newman, Holger Vömel, Karen Rosenlof, and Robert Portmann for helpful discussions. NCAR's Community Earth System Model project is supported primarily by the National Science Foundation. This material is based upon work supported by the National Center for Atmospheric Research, which is a major facility sponsored by the NSF under Cooperative Agreement No. 1852977. Computing and data storage resources, including the Cheyenne supercomputer (doi:10.5065/D6RX99HX), were provided by the Computational and Information Systems Laboratory (CISL) at NCAR.